INTERNATIONAL JOURNAL FOR NUMERICAL METHODS IN FLUIDS, VOL. 22, 121–135 (1995)

AN EXPLICIT FINITE VOLUME SPATIAL MARCHING METHOD FOR REDUCED NAVIER–STOKES EQUATIONS

K. SRINIVAS

Department of Aeronautical Engineering, University of Sydney, N.S.W. 2006, Australia

SUMMARY

This paper develops a spatial marching method for high-speed flows based on a finite volume approach. The method employs the reduced Navier–Stokes equations and a pressure splitting in the streamwise direction based on the Vigneron strategy. For marching from an upstream station to one downstream the modified five-level Runge–Kutta integration scheme due to Jameson and Schmidt is used. In addition, for shock handling and for good convergence properties the method employs a *matrix* form of the artificial dissipation terms, which has been shown to improve the accuracy of predictions. To achieve a fast rate of convergence, a local time-stepping concept is used. The method retains the time derivative in the governing equations and the solution at every spatial station is obtained in an iterative manner.

The developed method is validated against two test cases: (a) supersonic flow past a flat plate; and (b) hypersonic flow past a compression corner involving a strong viscous–inviscid interaction. The computed wall pressure and wall heat transfer coefficients exhibit good general agreement with previous computations by other investigators and with experiments.

KEY WORDS: spatial marching methods; reduced Navier–Stokes equations; explicit methods; Runge–Kutta method; hypersonic flow; supersonic flow

1. INTRODUCTION

Many of the practical flows of interest are complex and three-dimensional. The search for efficient methods to compute them continues. Time-marching methods have been widely used for the purpose, especially for compressible flows. Using these methods, one advances the solution at every point in a domain over several time steps or iterations until convergence or a steady state solution is reached. Such a procedure requires substantial computing time, especially for three-dimensional flows. However, if one considers supersonic or hypersonic flows with a dominant direction, spatial marching methods seem to be effective and more efficient.[1–5] Here one makes use of spatial stations (lines along which $x =$ const. in a typical two-dimensional flow) and marches from one station to the next one downstream, obtaining convergence at each. These methods are found to be almost an order of magnitude faster than time-marching methods[6] and this is seen to be a big advantage in computing three-dimensional flows.

Spatial marching methods exploit an important property of high-speed flows that any upstream influence in them is limited to thin boundary layer regions, leading to a substantial simplification of the computing procedure. Further, the usage of *reduced/parabolized Navier–Stokes (RNS) equations*, which are obtained by dropping the streamwise viscous terms from the Navier–Stokes equations, is another characteristic feature of these methods.

Realizing their advantages, there has been considerable progress in the development of spatial marching methods.[1–9] For a comprehensive review of these methods the reader is referred to Reference

CCC 0271–2091/96/020121–17

Received December 1993
Revised June 1994

1. Considering some of the previous works closely related to the present study, Lawrence *et al.*[2] have employed an upwind algorithm based on Roe's scheme[10] to compute two-dimensional flow fields. The method is implicit and second-order-accurate in the non-marching direction. Korte and McRae[3] also employ Roe's flux difference splitting, but their method is explicit and uses the MacCormack[11] scheme for marching. Both two- and three-dimensional flows have been computed using the resulting method. Siclari and Del Guidice[5] employ a semi-finite volume approach based on the Runge–Kutta scheme to compute three-dimensional inviscid flows. Harvey *et al.*[7] use solution-adapted grids with the flow solver developed by Lawrence *et al.*,[2] while Chang and Merkle[8] bring out the relationship between flux-vector-splitting and parabolized schemes. An analysis of the errors and convergence characteristics of iterative schemes for spatial marching is carried out in Reference 12.

Most of the spatial marching methods use implicit algorithms to march the solution. In contrast, the present author has been developing an explicit method for two-dimensional flows.[4,13,14] The method uses the modified Runge–Kutta scheme due to Jameson and Schmidt[15] to march the solution from an upstream station to a downstream one. It is characterized by the fact that the time derivative term in the governing equation is not dropped as is usual with spatial marching methods. Instead, the time step term Δt acts as a relaxation parameter, thus bringing the method within the *iterative* category.[12] In the earlier versions of the method a finite difference strategy was used along with artificial dissipation terms patterned after Jameson and Schmidt.[15] The method has been applied to compute shock–boundary layer interaction in a supersonic flow[4] and hypersonic flow past compression corners[13,14] with encouraging results.

The advantages of using an explicit method have been well-documented in the literature (see e.g. Reference 3). It must be pointed out that these methods do have disadvantages—time step limitation and the consequent large CPU time requirement being the most important. However, the speed of convergence does improve when the explicit methods are used in conjunction with available convergence acceleration devices.

The present method differs from the one described previously[4,13,14] in many ways. Here we employ a finite volume approach to carry out the computations entirely in the physical plane and avoid the calculation of the Jacobians of the transformation. The other important feature of the work is the implementation of a *matrix* form of the artificial dissipation terms, which has been shown to be effective in improving the accuracy of predictions, especially for high-speed flows.[16]

In the present work the spatial marching method has been applied to compute two test cases frequently used to validate the codes. The first deals with supersonic flow at Mach 2 along a flat plate[2] and the second is the well-known test case involving Mach 14·1 flow past a 15° compression corner due to Holdern and Moselle.[17]

The outline of the rest of the paper is as follows. Section 2 discusses the governing equations. The computational method employed is presented in detail in Section 3. The test cases, boundary conditions and computed results are discussed in Section 4 along with grid convergence studies for the hypersonic flow problem.

2. GOVERNING EQUATIONS

The governing equations are the two-dimensional, unsteady form of the Navier–Stokes equations. In Cartesian co-ordinates they are written as

$$\frac{\partial W}{\partial t}+\frac{\partial(F_{\rm i}-F_{\rm v})}{\partial x}+\frac{\partial(G_{\rm i}-G_{\rm v})}{\partial y}=0, \tag{1}$$

where

$$W = \begin{Bmatrix} \rho \\ \rho u \\ \rho v \\ e \end{Bmatrix}, \qquad F_{\rm i} = \begin{Bmatrix} \rho u \\ p + \rho u^2 \\ \rho uv \\ (e+p)u \end{Bmatrix}, \qquad G_{\rm i} = \begin{Bmatrix} \rho v \\ \rho uv \\ p + \rho v^2 \\ (e+p)v \end{Bmatrix}, \tag{2}$$

$$e = \frac{p}{\gamma - 1} + \tfrac{1}{2}\rho(u^2 + v^2), \qquad F_{\rm v} = \begin{Bmatrix} 0 \\ \sigma_{xx} \\ \tau_{xy} \\ u\sigma_{xx} + v\tau_{xy} - q_x \end{Bmatrix}, \qquad G_{\rm v} = \begin{Bmatrix} 0 \\ \tau_{xy} \\ \sigma_{yy} \\ u\tau_{xy} + v\sigma_{yy} - q_y \end{Bmatrix}, \tag{3}$$

$$\sigma_{xx} = \frac{\mu}{Re_\infty}\frac{2}{3}\left(2\frac{\partial u}{\partial x} - \frac{\partial v}{\partial y}\right), \qquad \sigma_{yy} = \frac{\mu}{Re_\infty}\frac{2}{3}\left(2\frac{\partial v}{\partial y} - \frac{\partial u}{\partial x}\right), \qquad \tau_{xy} = \frac{\mu}{Re_\infty}\left(\frac{\partial u}{\partial y} + \frac{\partial v}{\partial x}\right), \tag{4}$$

$$q_x = \frac{\mu}{Re_\infty}\frac{1}{(\gamma - 1)M_\infty^2 Pr}\frac{\partial T}{\partial x}, \qquad q_y = \frac{\mu}{Re_\infty}\frac{1}{(\gamma - 1)M_\infty^2 Pr}\frac{\partial T}{\partial y}. \tag{5}$$

The equations have been non-dimensionalized in the following manner (the dimensional quantities are denoted by a tilde):

$$t = \frac{\tilde t}{\tilde L \tilde U_\infty^2}, \quad x = \frac{\tilde x}{\tilde L}, \quad y = \frac{\tilde y}{\tilde L}, \quad u = \frac{\tilde u}{\tilde U_\infty}, \quad v = \frac{\tilde v}{\tilde U_\infty},$$
$$\rho = \frac{\tilde \rho}{\tilde \rho_\infty}, \quad T = \frac{\tilde T}{\tilde T_\infty}, \quad \mu = \frac{\tilde \mu}{\tilde \mu_\infty}, \quad p = \frac{\tilde p}{\tilde \rho_\infty \tilde U_\infty^2}, \tag{6}$$

where $\tilde L$ is the reference length. The freestream Reynolds number Re_∞ is given by $Re_\infty = \tilde\rho \tilde U_\infty \tilde L/\tilde\mu_\infty$. The coefficient of viscosity μ is calculated using the Sutherland equation

$$\mu = T^{3/2}\frac{1 + 110{\cdot}4/\tilde T_\infty}{T + 110{\cdot}4/\tilde T_\infty}.$$

Note that in the above expressions the Prandtl number Pr is assumed to be a constant. Further, the temperature is now given by $T = \gamma M_\infty^2 p/\rho$.

In accordance with the *RNS* approximation, the streamwise viscous terms are dropped while computing σ_{xx}, σ_{yy} and τ_{xy}.

2.1. Pressure splitting and evaluation of fluxes

The spatial marching methods are strictly valid for flows with no upstream influence. However, in viscous flows such as the ones considered here, there are subsonic portions of the boundary layer wherein the signals do propagate upstream. As a consequence, the spatial marching solution procedure is not well-posed and what are called *departure solutions* may result. Various methods have been suggested in the literature to suppress these solutions. Of these we employ the Vigneron pressure-splitting technique.[18] The splitting for the present application (i.e. a finite volume one) may be described as follows.

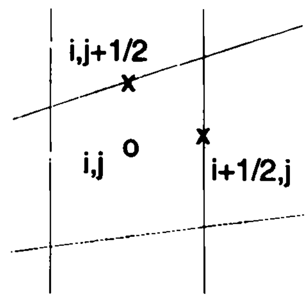

Figure 1. Typical finite volume

Consider a typical control volume set-up as shown in Figure 1. To implement the finite volume procedure, one has to determine the fluxes at the interfaces of the cell and its neighbours, i.e. at a location such as $(i+\frac{1}{2}, j)$. Usually this is done by first calculating the value of W as an average in the form $W_{i+1/2,j} = \frac{1}{2}(W_{i,j} + W_{i+1,j})$. However, in spatial marching procedures, where the fluxes in the marching direction are upwinded, we have $W_{i+1/2,j} = W_{i,j}$ and the pressure at the interface is determined as

$$P_{i+1/2,j} = \omega p_{i,j} + (1-\omega)p_{i+1,j}, \tag{7}$$

where the parameter ω is given by

$$\omega = \min\left[1, \frac{\sigma\gamma M_\xi^2}{1+(\gamma-1)M_\xi^2}\right]. \tag{8}$$

Here M_ζ is the local streamwise Mach number, while σ is a factor that takes into account the non-linearities not included in the analysis[2] and is taken as 0·7 in the present work. Further, the term $(1-\omega)p_{i+1,j}$ in (7) is to account for any upstream influence in the subsonic portions of boundary layers. The present method employs a single sweep through the domain and accordingly this term is dropped.

In the non-marching direction, i.e. at the top and bottom faces of the cell (say at $(i, j+\frac{1}{2})$), the fluxes are evaluated by averaging the values of W of the adjacent cells (i.e. j and $j+1$). Note that the pressure splitting influences the inviscid fluxes only. The required viscous fluxes across the cell faces are computed directly in the physical plane by evaluating the first derivatives (e.g. $\partial T/\partial y$) in a typical finite volume manner.

3. COMPUTATIONAL METHOD

The first step in the numerical solution procedure consists of reducing the given governing equation to an ordinary differential equation by choosing a suitable discretization for the spatial derivatives, which for the present case may be described as follows. Consider a typical finite volume as shown in Figure 1. If Q denotes the flux through any of the faces of the control volume and A denotes the area (of the control volume), then the governing equation (1) reduces to

$$\frac{\mathrm{d}}{\mathrm{d}t}(AW) + \sum_{nn=1}^{nn=4} Q(F, G) = 0, \tag{9}$$

where the summation is over the faces of the control volume (see Figure 1). We apply the modified Runge–Kutta method[15] to solve the above equation. It may be pointed out that in spatial marching applications it is usual to drop the $d(AW)/dt$ term in (9). However, we retain the term and integrate the above equation at every spatial station. Thus in the present procedure, at any spatial station i, $W(i,j)$ is first set equal to $W(i-1,j)$ for every cell in the j-direction (i.e. the non-marching direction) and the solution is iterated using equation (9) till a convergence criterion (described later) is satisfied. In effect, the time step term Δt behaves like an iteration parameter and is calculated according to[19]

$$\frac{\Delta t}{A}=\frac{CFL}{|\Delta xv-\Delta yu|+a\sqrt{(\Delta x^2+\Delta y^2)}+4\gamma\mu(\Delta x^2+\Delta y^2)/A\,Pr\,\rho}. \tag{10}$$

The modified Runge–Kutta method may be summarized as follows. If W^n is the solution at $t=t_0$, then W^{n+1}, the solution at $t_0+\Delta t$, i.e. after one iteration, is given by (indices i and j omitted for convenience)

$$\begin{aligned}
W^{(0)}&=W^n,\\
W^{(1)}&=W^{(0)}-\alpha^{(1)}\Delta t[Q(W^{(0)})],\\
&\;\vdots\\
W^{(k)}&=W^{(0)}-\alpha^{(k)}\Delta t[Q(W^{(k-1)})],\\
W^{n+1}&=W^{(k)},
\end{aligned} \tag{11}$$

where k is the number of levels used in the integration procedure. The present work has $k=5$ and the coefficients α are $\frac{1}{4}$, $\frac{1}{6}$, $\frac{3}{8}$, $\frac{1}{2}$ and 1.

3.1. *Artificial dissipation*

For stability near shocks and for better convergence properties the present method needs artifical dissipation and this is provided in a flow-adapted manner.[15] Accordingly, equation (9) is replaced by

$$\frac{d}{dt}(AW)+\sum_{nn=1}^{nn=4}[Q(F,G)-D]=0. \tag{12}$$

The dissipation term D in the above equation is a blend of second- and fourth-order differences and is required only in the non-marching direction in the present application. For the interface between cells (i,j) and $(i,j+1)$ it is given by (index i has been suppressed)

$$\begin{aligned}
DW_{j+1/2}&=(d^{(2)}-d^{(4)})W_j,\\
d^{(2)}W_{j+1/2}&=(\lambda_{j+1/2}\varepsilon^{(2)}_{j+1/2}\Delta_y)W_j,\\
d^{(4)}W_{j+1/2}&=[(\lambda_{j+1/2}\varepsilon^{(4)}_{j+1/2})\Delta_y\nabla_y\Delta_y]W_j,
\end{aligned} \tag{13}$$

where λ is proportional to the spectral radius of the Jacobian matrix ($-\Delta y\partial F/\partial W+\Delta x\partial G/\partial W$, where Δx and Δy are the intercepts made by the cell face upon the co-ordinate axes), Δ_y and ∇_y are the forward and backward differences in the y-direction respectively and $\varepsilon^{(2)}$ and $\varepsilon^{(4)}$ are the flow-adapted coefficients defined in Reference 16. This form is termed a *scalar* model of dissipation, taking into account that λ is a scalar, and was the one used in the previous versions of the present method. It may be observed that the dissipation needed for each of the governing equations is scaled with the same factor λ. The results obtained using this model were generally good but the resolution of some of the important features of the flow seemed inadequate.[14] To improve the predictions, this form of dissipation is now replaced by a *matrix* form where a matrix (closely related to the Jacobain matrix) is used in place of λ. The studies by Swanson and Turkel[16] and Swanson *et al.*[19] indicate that the accuracy of predictions and the resolution of flow features are substantially better with the matrix form, especially at high Mach numbers. A brief description of this form is given below and details can be found in the above references.

The most important change in the artificial dissipation terms consists of replacing the λ term in (13) by

$$T|\Lambda|T^{-1}, \tag{14}$$

where

$$T = \begin{bmatrix} 1 & 0 & \beta & \beta \\ u & \kappa_y \rho & \beta(u + \kappa_x a) & \beta(u - \kappa_x a) \\ v & -\kappa_y \rho & \beta(v + \kappa_y a) & \beta(v - \kappa_y a) \\ \dfrac{\psi}{\gamma - 1} & \rho(\kappa_y u - \kappa_x v) & \beta\left(\dfrac{\psi + a^2}{\gamma - 1} + a\theta\right) & \beta\left(\dfrac{\psi + a^2}{\gamma - 1} - a\theta\right) \end{bmatrix}, \tag{15}$$

$$T^{-1} = \begin{bmatrix} 1 - \dfrac{\psi}{a^2} & \dfrac{\gamma - 1}{a^2} u & \dfrac{\gamma - 1}{a^2} v & -\dfrac{\gamma - 1}{a^2} \\ \dfrac{-(\kappa_y u - \kappa_x v)}{\rho} & \dfrac{\kappa_y}{\rho} & -\dfrac{\kappa_y}{\rho} & 0 \\ \phi(\psi - a\theta) & \phi[\kappa_x a - (\gamma - 1)u] & \phi[\kappa_y a - (\gamma - 1)v] & \phi(\gamma - 1) \\ \phi(\psi + a\theta) & -\phi[\kappa_x a + (\gamma - 1)u] & -\phi[\kappa_y a + (\gamma - 1)v] & \phi(\gamma - 1) \end{bmatrix}. \tag{16}$$

In the above equations a is the speed of sound and u and v are the average velocity components on the cell face. The other terms in the equations are given by

$$\beta = \frac{\rho}{\surd 2a}, \qquad \kappa_x = \frac{-\Delta y}{\surd(\Delta x^2 + \Delta y^2)}, \qquad \kappa_y = \frac{\Delta x}{\surd(\Delta x^2 + \Delta y^2)},$$
$$\theta = \kappa_x u + \kappa_y v, \qquad \phi = \frac{1}{\surd 2\rho a}, \qquad \psi = \tfrac{1}{2}(\gamma - 1)(u^2 + v^2).$$

The significance of the terms T and T^{-1} lies in that these contribute to the similarity relationship

$$-\Delta y \frac{\partial F}{\partial W} + \Delta x \frac{\partial G}{\partial W} = TEVT^{-1},$$

where EV is a diagonal vector of the eigenvalues, which for the present governing equations are Vc, Vc, $Vc + a\surd(\Delta x^2 + \Delta y^2)$ and $Vc - a\surd(\Delta x^2 + \Delta y^2)$. Here Vc is the flux velocity given by $Vc = -\Delta yu + \Delta xv$. The matrix form of the dissipation replaces EV by

$$\Lambda = \mathrm{diag}(\tilde{\lambda}_1, \tilde{\lambda}_2, \tilde{\lambda}_3, \tilde{\lambda}_4), \tag{17}$$

where

$$\begin{aligned} \tilde{\lambda}_1 &= \max[|Vc|, \zeta \cdot \Pi], & \tilde{\lambda}_2 &= \max[|Vc|, \zeta \cdot \Pi], \\ \tilde{\lambda}_3 &= \max[|Vc + a\surd(\Delta x^2 + \Delta y^2)|, \zeta \cdot \Pi], & \tilde{\lambda}_4 &= \max[|Vc - a\surd(\Delta x^2 + \Delta y^2)|, \zeta \cdot \Pi]. \end{aligned} \tag{18}$$

Here $\Pi = |Vc| + a\surd(\Delta x^2 + \Delta y^2)$ is the maximum eigenvalue. Thus we see that the dissipation for each of the governing equations is scaled with a $\tilde{\lambda}$ which is the greater of the eigenvalue for the equation and ζ times the maximum eigenvalue; ζ is a coefficient chosen to give a good definition of

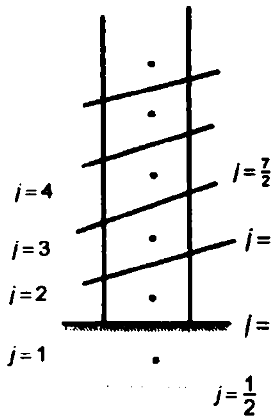

Figure 2. Finite volume cells near the boundary

flow features such as shocks and for good convergence and is set equal to 0·2 in the present application.

The other important terms in (13) are given by

$$\varepsilon^{(2)}_{j+1/2} = \frac{|p_{j+1} - 2p_j + p_{j-1}|}{(1 - \bar{\omega}(|p_{j+1} - p_j| + |p_j - p_{j-1}|) + \bar{\omega}|p_{j+1} + 2p_j + p_{j-1}|},$$

$$\varepsilon^{(4)}_{j+1/2} = \max[0, k^{(4)} - \varepsilon^{(2)}_{j+1/2}]. \tag{19}$$

It may be pointed out that in (19) the term $\varepsilon^{(2)}$ is zero in regions where the pressure distribution is uniform and non-zero in regions where there is a strong pressure gradient. Thus the term $d^{(2)}$ in (13) is activated near shocks and similar features. The influence of $\bar{\omega}$ in (19) is discussed in Reference 16 and it is chosen to give a good definition of shocks (the present application used a value of $\frac{1}{2}$). The parameter $k^{(4)}$ is about $\frac{1}{16}$ and is chosen for good convergence of the solution. Another feature that can influence the convergence properties of the method is the manner in which the differences that make up the artificial dissipation terms near the boundaries are calculated. In this study we follow the suggestions in Reference 16 and impose (see Figure 2)

$$(\Delta W)_{j=1/2} = 2(\Delta W)_{j=3/2} - (\Delta W)_{j=5/2}. \tag{20}$$

It may be noted that the boundary conditions determine the flow variables at the location $j = 1$. The artificial dissipation terms are further weighted by a factor γ_m as detailed in Reference 20 and are evaluated after the first, third and fifth stages of the Runge–Kutta scheme (see equation (11)).

4. RESULTS AND DISCUSSION

The spatial marching method developed in the previous sections is applied to compute two test cases: (a) supersonic flow over a flat plate; (b) hypersonic flow past a compression corner. Both flows are two-dimensional and laminar and in both flows the wall temperature is held constant. Each of these flows was computed by starting with freestream conditions at $x = 0$ and marching downstream. Very fine steps (Δx about 0·0001) were taken close to the leading edge for both problems and near the corner as well for the hypersonic flow problem. At the other locations the spatial steps taken were much coarser and uniform. For both problems the grid in the flow normal direction was stretched, with the first cell close to the wall being about 0·0001 m high, the number of cells being 45 for flow (a) and 65 for flow (b).

At each station the term Δt (equation (11)) was varied from cell to cell, which corresponds to the use of a *local time step*. The magnitude of the *time step* chosen corresponded to maximum possible Courant numbers (*CFL* in (10)). It was found that stable computations were possible with a Courant number of 3·0 for the flat plate problem and 1·0 for the compression corner flow. At every station a number of iterations were carried out till the RMS change in density between successive iterations was below 0·0001.

The boundary conditions employed were the standard ones. At the solid wall boundary for both problems a no-slip condition ($u = v = 0$) was imposed together with a zero-order extrapolation of pressure. The wall temperature was forced to be equal to T_{wall} and the subsequent wall density calculated. At the freestream boundary all the variables were set equal to their freestream values (i.e. $u_\infty, v_\infty, p_\infty, \rho_\infty$).

The results obtained for the two test cases are presented and discussed in the following subsections.

4.1. Supersonic flow past a flat plate

The test case involves a supersonic flow past a flat plate with a thin leading edge. Features of the flow consist of a weak leading edge shock and a laminar boundary layer and the test case is intended to bring out the capability of the method to handle the viscous effects. The freestream conditions are $M_\infty = 2{\cdot}0$, $Re_\infty/\bar{L} = 1{\cdot}65 \times 10^6\ \text{m}^{-1}$, $\tilde{T}_\infty = \tilde{T}_{\text{wall}} = 221{\cdot}6$ K, $Pr = 0{\cdot}72$ and $\gamma = 1{\cdot}4$. Computations were carried out starting from the leading edge ($x = 0$) for a plate length of unity.

Computed tangential velocity (u) and temperature (T) profiles at $\bar{X} = 0{\cdot}915$ m are shown in Figures 3 and 4 respectively. The profiles are compared with those obtained by Lawrence *et al.*[2] using an upwind algorithm based on Roe's scheme. There is overall agreement between the two results. However, the present results tend to underpredict the velocities in comparison with Lawrence *et al.*[2] At the same time the peak temperature predicted close to the wall is slightly lower.

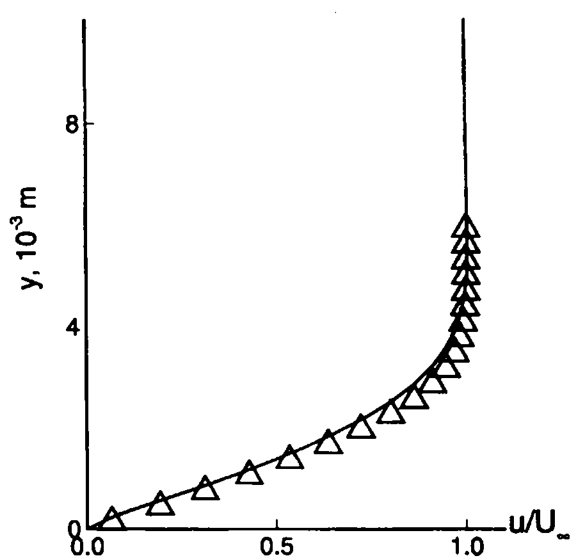

Figure 3. Computed tangential velocity profile for supersonic flow at $\bar{x} = 0{\cdot}915$ m: —, present; Δ, Lawrence *et al.*[2]

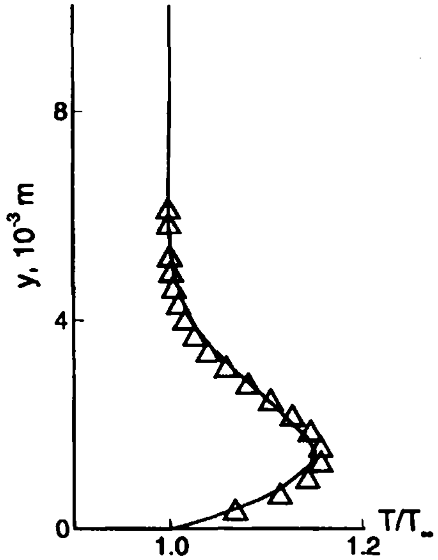

Figure 4. Computed temperature profile for supersonic flow at $\bar{x} = 0{\cdot}915$ m: —, present; Δ, Lawrence *et al.*[2]

Figure 5 compares the distribution of the wall heat transfer coefficient defined as

$$C_h = \frac{\mu_{\text{wall}}}{Pr\,Re_\infty} \frac{1}{\frac{1}{2}(\gamma - 1)M_\infty^2 + 1 - T_w} \frac{\partial T}{\partial n}, \tag{21}$$

where n denotes the distance normal to the wall. The present method is observed to give slightly higher values than Lawrence *et al.*[2]

It is clear that the present method is capable of handling well the viscous effects in a supersonic flow. The departure of the present results from those of Lawrence *et al.*[2] is perhaps explained by the difference in the starting conditions used in the two studies.

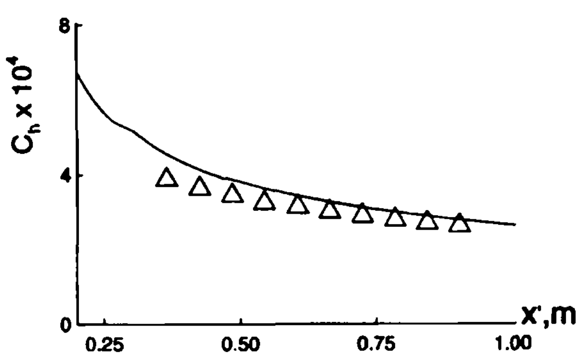

Figure 5. Distribution of wall C_h for supersonic flow: —, present; Δ, Lawrence *et al.*[2]

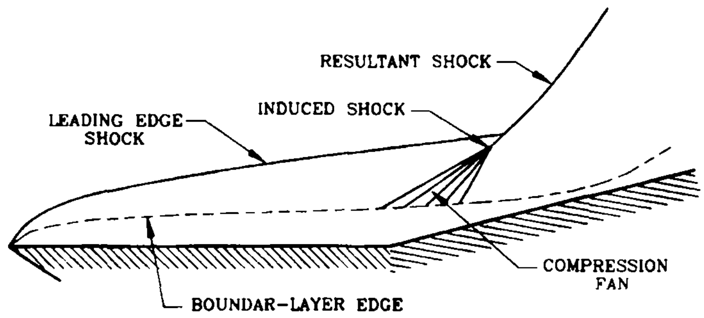

Figure 6. Hypersonic flow test case

4.2. Hypersonic flow past a compression corner

This is a very frequently studied computational test case[2,3,6,14,19,21] for which the experimental results are also available[17] and involves a Mach 14·1 flow negotiating a 15° compression corner. The flow is schematically sketched in Figure 6 and involves a strong viscous–inviscid interaction but no separation. Owing to the high freestream Mach number, there is a pressure gradient across the boundary layer and a leading edge shock. This shock interacts with the compression shock at the corner, resulting in a stronger shock, expansion and a slip surface. In addition, there is a thinning of the boundary layer due to compression and a consequence increase in pressure and heat transfer following the corner. Thus it is a challenge for any code to predict all these features accurately. The freestream conditions for this test case are $M_\infty = 14{\cdot}1$, $Re_\infty/\tilde{L} = 1{\cdot}04 \times 10^6\ \mathrm{m}^{-1}$, $\tilde{L} = 0{\cdot}439$ m, $\tilde{T}_\infty = 72{\cdot}2$ K, $\tilde{T}_{\mathrm{wall}} = 297{\cdot}0$ K and $Pr = 0{\cdot}72$. The freestream temperature is low and real gas effects are not expected to be significant.

Computations for this test case started at the leading edge $x = 0$ and were carried out till the downstream station $x = 2$ was reached. The marching method was found to be stable only for values of *CFL* (equation (10)) below unity in regions downstream of the corner. This is probably because of the sharp rise in pressure that follows the shock interaction.

Many interesting features present in the flow along with a strong shock seem to make this example a good test case for carrying out grid convergence and other studies. Accordingly, it was computed with many different grids and the results are summarized below.

It was found that the results, particularly the C_h distribution, are sensitive to the grid spacing in both the x- and y-directions. In the x-direction (i.e. the marching direction) the spacing at the corner where the pressure undergoes a steep rise seems to be crucial. Figure 7 shows the effect of the grid spacing (Δx) at the corner on the heat transfer rate (C_h) distribution and it is clear that the distribution is grid-independent for Δx smaller than $0{\cdot}2 \times 10^{-2}$. Higher values of Δx very greatly influence the distribution. In the y-direction it is observed that (Figure 8) grid independence is achieved for Δy smaller than 6×10^{-4}. The other feature of interest, namely the C_p distribution along the wall, seemed less sensitive to the grid spacing. Convergence histories at a few of the spatial stations are shown in Figure 9. As expected, fast convergence is obtained in the flat plate region of the flow closer to the leading edge ($x = 0{\cdot}2$) and in regions far downstream of the corner ($x = 1{\cdot}8$). However, in the vicinity of the corner ($x = 1{\cdot}02$ and $1{\cdot}1$) it takes many more iterations to converge. These computations required about 1 h CPU time on an IBM RISC-6000 machine.

The grid-independent results obtained for this flow are compared with experiments, those obtained with a scalar form of artifical dissipation and those of other investigators and discussed below.

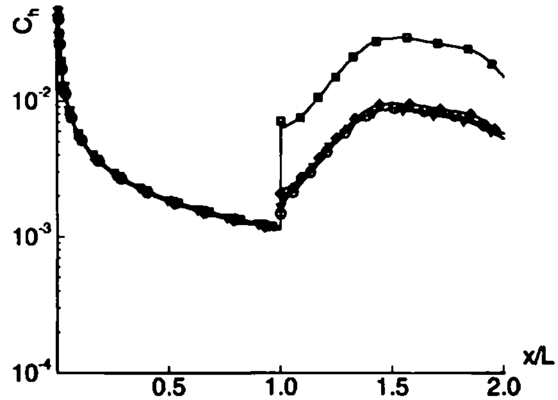

Figure 7. Distribution of wall C_h for various values of Δx at the corner: □, $\Delta x = 0{\cdot}4 \times 10^{-2}$; ◇, $\Delta x = 0{\cdot}2 \times 10^{-2}$; ○, $\Delta x = 0{\cdot}1 \times 10^{-2}$; ▽, $\Delta x = 0{\cdot}66 \times 10^{-3}$

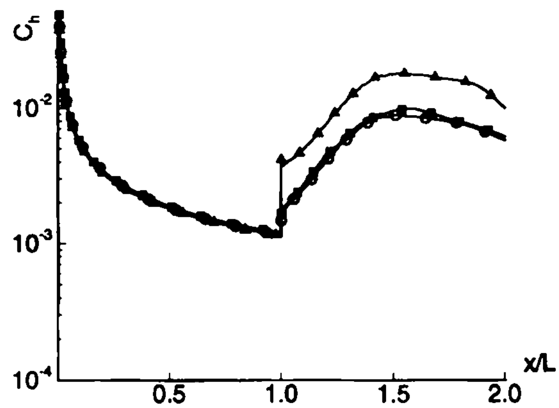

Figure 8. Distribution of wall C_h for various values of Δy at the wall: △, $\Delta y = 0{\cdot}8 \times 10^{-4}$; □, $\Delta y = 0{\cdot}6 \times 10^{-4}$; ○, $\Delta y = 0{\cdot}4 \times 10^{-4}$

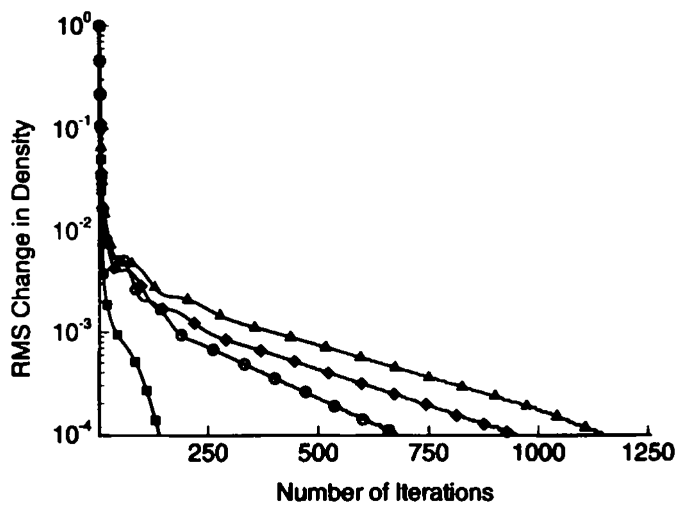

Figure 9. Convergence history: □, at $x = 0{\cdot}2$; ○, at $x = 1{\cdot}8$; △, at $x = 1{\cdot}02$; ◇, at $x = 1{\cdot}1$

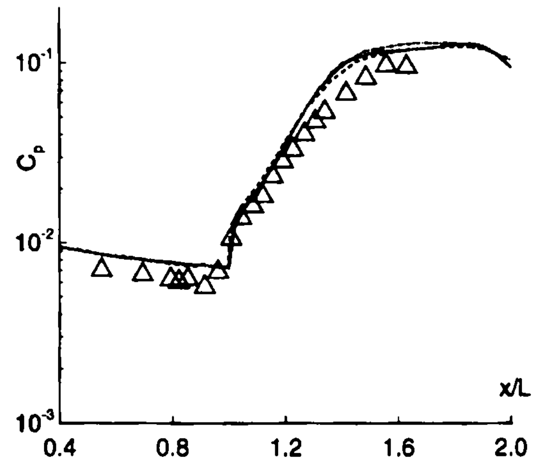

Figure 10. Wall C_p distribution for hypersonic flow test case: —, present with matrix dissipation; —·—·—, present with scalar dissipation; ----, second-order Roe scheme;[2] △, Holden and Moselle[17]

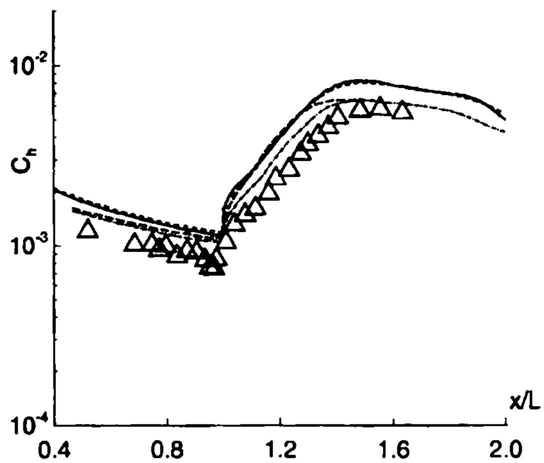

Figure 11. Wall C_h distribution for hypersonic flow test case; —, present with matrix dissipation; ----, present with scalar dissipation; — — —, first-order Roe scheme;[2] —·—·—, second-order Roe scheme;[2] △, Holden and Moselle[17]

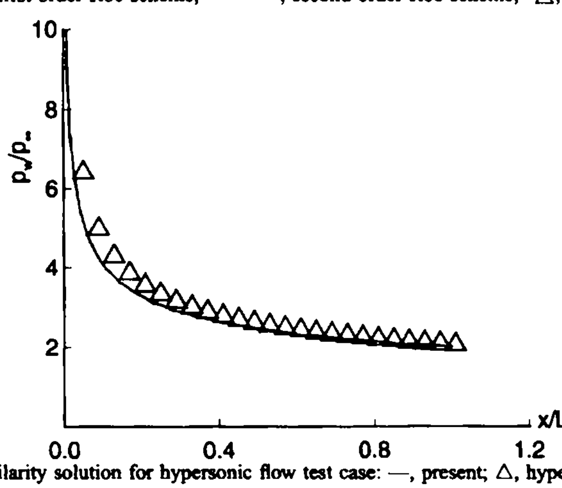

Figure 12. Similarity solution for hypersonic flow test case: —, present; △, hypersonic similarity

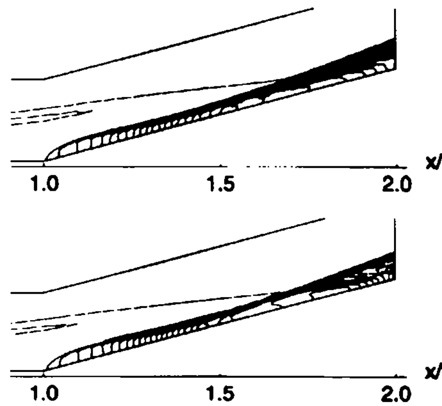

Figure 13. Computed C_p contours for hypersonic flow test case (contour interval 0·01): top; using scalar form of artificial dissipation; bottom, using matrix form of artifical dissipation

Figures 10 and 11 compare the computed wall pressure coefficient (defined as $C_p = p_{wall}/\rho_\infty U_\infty^2$) and wall heat transfer coefficient C_h respectively. Upsteam of the corner the experimental results show a *dip*, which is typically due to the upstream influence which the present spatial marching method does not handle. However, this dip does not seem to influence the solution in other regions of the flow. The general trends in the two distributions are captured well, including the position where the maximum C_p or C_h occurs after the corner. However, there is an overprediction of both these coefficients even in the flat plate region upstream of the corner. It may be pointed out that such an overprediction occurs even in the results of Lawrence *et al.*,[2] Korte and McRae[3] and Harvey *et al.*[7] It is worth noting that Rudy *et al.*[21] were able to obtain better agreement with experiments after introducing an angle-of-attack correction.

The form of the artificial dissipation terms used (scalar or matrix) does not seem to influence substantially the C_h distribution or the C_p distribution. Comparing the present results with those of Lawrence *et al.*[2] who have used Roe's first- and second-order schemes,[10] we observe good agreement in the C_p distribution. However, the C_h distribution indicates that the present method overpredicts the heat transfer rates.

A check was made in the present study to find out how far the present results agreed with the hypersonic similarity solution. The theoretical pressure distribution along the flat portion of the geometry was calculated using the similarity principle[22] and is compared with the present results in Figure 12. Good agreement is evident, suggesting that the conditions in the experiments may not have been strictly two-dimensional.

Figures 13 and 14 show the contours of C_p (drawn at 0·01 intervals) and Mach number (drawn at 0·5 intervals) for the flow respectively. The C_p contours clearly reveal the interaction, showing the resulting shock and expansion fan. The Mach number contours clearly show that slip surface produced after the interaction. These results are seen to be markedly better than the ones given by the earlier version of the method using a scalar form of artificial dissipation, which tends to smear quite a few of the details.

Thus is seems that the present method is capable of adequately resolving the features of a strong hypersonic interaction. The method, though tested here for two-dimensional flows, is expected to be very efficient for three-dimensional flows.

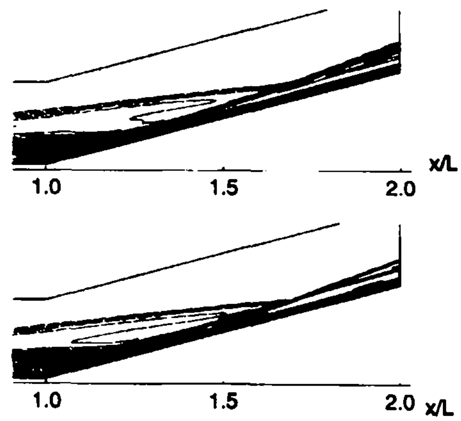

Figure 14. Computed Mach number contours for hypersonic flow test case (contour interval 0·5): top, using scalar form of artificial dissipation; bottom, using matrix form of artificial dissipation

5. CONCLUSIONS

A spatial marching method using the Runge–Kutta integration scheme has been developed for high-speed flows. Utilizing finite volumes, the method solves the Reduced Navier–Stokes equations. For stability near shocks and to improve the convergence behaviour, a *matrix* form of the dissipation terms is employed. Two test cases were computed using the method and the computed results are in agreement with other computed and experimental results. The method is expected to be very efficient for three-dimensional flows.

ACKNOWLEDGEMENTS

Thanks are due to Dr. D. J. Auld, Mr. D. M. Newman and Mr. C. Mellen for their help in the production of the manuscript.

APPENDIX: NOMENCLATURE

A	area
C_h	heat transfer coefficient
C_p	coefficient of pressure
$d^{(2)}$, $d^{(4)}$	terms in expression for dissipation
D	dissipation term
e	total energy
F_i, F_v	inviscid and viscous fluxes in x-direction
G_i, G_v	inviscid and viscous fluxes in y-direction
i	index to denote marching direction
j	index to denote non-marching direction
k	coefficient in Runge–Kutta procedure
M_ζ	local streamwise Mach number
M_∞	freestream Mach number
p	pressure
Pr	Prandtl number
q_x, q_y	heat transfer terms in x- and y-directions

Re_∞	freestream Reynolds number
T	temperature
u, v	velocity components in x- and y-directions
W	array defined in equation (1)

Greek letters

μ	viscosity
σ_{xx}, σ_{yy}, τ_{xy}	stress components
ρ	density

REFERENCES

1. S. G. Rubin and J. C. Tannehill, 'Parabolized/reduced Navier–Stokes computational techniques', *Ann. Rev. Fluid Mech.*, **24**, 117–144 (1992).
2. S. L Lawrence, J. C. Tannehill and D. S. Chausee, 'Upwind algorithm for the parabolized Navier–Stokes equations', *AIAA J.*, **27**, 1175–1183 (1989).
3. J. J. Korte and D. S. McRae, 'Explicit upwind algorithm for the parabolized Navier–Stokes equations', *AIAA Paper 88-0176*, 1988.
4. K. Srinivas, 'An explicit spatial marching algorithm for Navier–Stokes equations', *Comput. Fluids*, **21**, 291–299 (1992).
5. M. J. Siclari and P. Del Guidice, 'Hybrid finite volume approach to Euler solutions for supersonic flows', *AIAA J.*, **28**, 66–74 (1990).
6. R. W. Newsome, R. W. Walters and J. L. Thomas, 'Iteration strategy for upwind/relaxation solutions to the thin-layer Navier–Stokes equations', *AIAA J.*, **27**, 1165–1166 (1989).
7. A. D. Harvey III, S. Acharya, S. L. Lawrence and S. Cheung, 'Solution-adaptive grid procedure for high-speed parabolic flow solvers', *AIAA J.*, **29**, 1232–1240 (1991).
8. C. L. Chang and C. L. Merkle, 'The relation between flux vector splitting and parabolized schemes', *J. Comput. Phys.*, **80**, 344–361 (1989).
9. T. Chitsomboon, A. Kumar and S. N. Tiwari, 'A parabolized Navier–Stokes algorithm for separated supersonic internal flows', *AIAA Paper 85-1411*, 1985.
10. P. L. Roe, 'Approximate Riemann solvers, parameter vectors and difference schemes', *J. Comput. Phys.*, **43**, 357–372 (1981).
11. R. W. MacCormack, 'The effect of viscosity in hypervelocity impact crating', *AIAA Paper 69-354*, 1969.
12. D. S. Thompson and R. J. Matus, 'Conservation errors and convergence characteristics of iterative space-marching algorithms', *AIAA J.*, **29**, 227–234 (1991).
13. K. Srinivas, 'Computation of hypersonic flow past a compression corner by a spatial marching scheme', in R. Abgrall, J. A. Desideri, R. Glowinski, M. Mallet and J. Periaux (eds), *Hypersonic Flows for Reentry Problems*, Vol. 3, Springer, New York, 1992, pp. 338–341.
14. K. Srinivas, 'Computation of high speed flows using an explicit spatial marching algorithm', in M. R. Davis and G. J. Walker (eds), *Proc. 11th Australasian Fluid Mechanics Conf.*, Hobart, December 1992, pp. 711–714.
15. A. Jameson and W. Schmidt, 'Some recent developments in numerical methods for transonic flows', *Proc. FENOMECH '84 conf.*, Stuttgart, September 1984.
16. R. C. Swanson and E. Turkel, 'On central-difference and upwind schemes', *J. Comput. Phys.*, **101**, 292–306 (1992).
17. M. S. Holden and J. R. Moselle, 'Theoretical and experimental studies of shock wave boundary layer interaction on compression surfaces in hypersonic flow', *Rep. AF-24110-A-1*, CALSPAN, Buffalo, NY. 1969.
18. Y. C. Vigeron, J. V. Rakich and J. C. Tannehill, 'Calculation of supersonic viscous flow over delta wings and sharp subsonic leading edges', *AIAA Paper 78-1137*, 1978.
19. R. C. Swanson, E. Turkel and J. A. White, 'An effective multigrid method for high-speed flows', Commun. Appl. Numer. Methods, **8**, 671–681 (1992).
20. R. C. Swanson and R. Radespiel, 'Cell centered and cell vertex multigrid schemes for the Navier–Stokes equations', *AIAA J.*, **29**, 697–703 (1991).
21. D. H. Rudy, A. Kumar, J. L. Thomas, P. A. Gnoffo and S. R. Chakravarthy, 'A validation study of four Navier–Stokes codes for high-speed flows', *AIAA Paper 89-1838*, 1989.
22. W. H. Dorrance, *Viscous Hypersonic Flow*, McGraw-Hill, New York, 1962.